A hybrid photogrammetry approach for archaeological sites: Block alignment issues in a case study (the Roman camp of *A Cidadela)*

Arza-García, M., Gil-Docampo, M., & Ortiz-Sanz, J.

Abstract

Photogrammetry is a cost-effective and versatile technique used for the three-dimensional (3D) registration of archaeological heritage sites. Managing datasets of heterogeneous images in terms of camera type, elevation platform, position or acquisition time can now be addressed by structure from motion (SfM) software via bundle adjustment in a single block based on collinearity principles. This development enables new possibilities with regard to data completeness assurance for 3D documentation, even for complex sites with occlusive elements and hidden areas. However, hybrid photogrammetry in large datasets often requires multiple photogrammetric blocks that must be processed individually and subsequently aligned to obtain a unified point cloud. In this paper, we discuss the steps required to homogenize the information and the methods used to perform block alignment in these cases. A case study of low-altitude aerial photogrammetry with several cameras and platforms is presented for the Roman camp of *A Cidadela* in NW Spain as a representative example of an archaeological site that is difficult to survey using a single photogrammetric platform. The relatively large expanse of the area and the fact that it is partially covered by a protective structure constitute an ideal framework for the fusion of multiplatform imagery. The most accurate digital surface model (DSM) was obtained via point-based method fusion, during which subsets are aligned based on automatically extracted tie points (TPs) between the dense point clouds; however, point-based method fusion is very time consuming. When hardware capabilities allow, conducting the process in a single block is preferable, which is a noticeably more accurate procedure than independent block fusion.

Keywords

1   Research Aims

This paper presents an overall pipeline for hybrid photogrammetry[1] and discusses the typical problems of integrating multiple photogrammetric sources; it focuses primarily on the analysis of the procedures used to perform block fusion to obtain a complete digital surface model (DSM) of an archaeological site, but it also includes recommendations (e.g., practical tips for image acquisition, procedures to homogenize data or radiometric post-processing) for situations in which multiple image sources must be integrated. Finally, an accuracy assessment is performed in the case of the Roman settlement of *A Cidadela* (NW Spain), whose complexity requires the use of multiple platforms (UAV and pole) and several camera types.

2   Introduction

The documentation of archaeological heritage is an essential task in terms of its study, dissemination, preservation and even reconstruction. Recently, several techniques have been employed for this purpose, but the use of laser scanning is considered to be one of the most precise for 3D recording (Senol *et al.*, 2017; Bermejo *et al.*, 2018).

However, the greatest revolution in the way cultural heritage is documented has been modern photogrammetry, as is evident in a wide range of studies (Green, Bevan and Shapland, 2014; Robleda *et al.*, 2015; Sapirstein, 2016). Like traditional stereoscopic photogrammetry, structure from motion (SfM) uses well-defined geometrical features

---

[1] The term "hybrid photogrammetry" is used in this context to refer to the fusion of multiplatform close-range photogrammetry. In this paper, we refer particularly to low-altitude aerial photogrammetry using a pole and UAV-based photogrammetry.

captured in multiple images from several angular viewpoints to generate a 3D point cloud (Westoby *et al.*, 2012). However, while traditional photogrammetry primarily derives the calibration parameters of the camera and the exterior orientation parameters from well-distributed ground control points (GCPs) and tie points (TPs), the SfM approach simultaneously computes both the relative projection geometry and a set of sparse 3D points (Chiabrando, Donadio and Rinaudo, 2015).

Modern photogrammetry based on automatic image correlation (AIC) algorithms enables significant automation of the process (Remondino *et al.*, 2013); however, automated software processes also impose high demands on the quality and geometric configuration of images (Tscharf *et al.*, 2015). In particular, complex object geometries and occlusive elements can pose problems for correlation algorithms. Moreover, because AIC requires high overlap and a very dense image network to guarantee completeness, the radiometric variations of objects in different images can generate matching fails. In this sense, an improvement in the results can be expected with the use of a uniform data source. However, in complex archaeological photogrammetric surveys, geometric requirements cannot be ensured by using one image source exclusively. Thus, in many cases, only the effective combination of multiplatform photogrammetry can guarantee completeness.

The SfM and AIC algorithms allow orientation parameters to be computed individually for each image, enabling the simultaneous processing of a large number of images with different positions or taken by different cameras (with varied focal lengths, image sizes, etc.) in a single block (Manferdini and Galassi, 2013). The increasing processing capabilities of new IT equipment reduce reconstruction times; however, larger batches of images are becoming increasingly common due to the use of massive capture systems such as unmanned aerial vehicles (UAVs), which have greatly reduced the work of large surveys (Arif and Essa, 2017; Campana, 2017; Field, Waite and Wandsnider, 2017). Thus, the trade-off between dataset size and processing capacity remains the main factor that determined whether to work with the entire dataset at once or to divide the images into several subsets (i.e., individual blocks; these blocks could be defined by other

names depending on the program used, such as "chunks" for Photoscan (Agisoft, Saint Petersburg, RU), "projects" for Pix4D (Pix4D SA, Lausanne, CH) and "components" for RealityCapture (Capturing Reality, Bratislava, SK)). Alignment is also essential is when adding an extra set of images to a block that is already aligned.

Because each individual point cloud is georeferenced by an independent bundle adjustment and separate workflows, there is the potential for misalignments between blocks. In this sense, SfM photogrammetry continues to inherit from classic photogrammetry the need to use subsequent methods of alignment to obtain an accurately merged block. Generally, this alignment process is performed using solid rigid transformations (e.g., simple rotations, translations or their combination) based on reference elements in one of the blocks that are used to obtain the coordinates of the homologous points in the other blocks. The methods mainly differ in terms of the reference elements used for this rigid transformation. Among the most common options implemented in commercial photogrammetry packages are the use of manually entered TPs, common images in different "chunks" or a dense set of homologous points (automatic TPs) extracted by matching between point clouds.

Merging photogrammetric sources is a very common procedure in many fields (Bemis *et al.*, 2014; Fugazza *et al.*, 2018), such as those related to cultural heritage (Bolognesi *et al.*, 2014; Seibert von Fock *et al.*, 2017). However, while independent block accuracy analysis is a frequently addressed subject (Nocerino *et al.*, 2013; Martínez-Carricondo *et al.*, 2018), the accuracy of the alignment procedures has not itself been extensively studied, probably due to a lack of knowledge of the internal workings of commercial software packages, which are essentially black boxes.

3   Materials and Method

3.1   Description of the study site

The camp of *A Cidadela* (43º 05´ N, 8º 02´ W, altitude 475 m MAMSL) is located in Sobrado dos Monxes (A Coruña) in northwest Spain. This Roman structure sits on a plateau and consists of a military camp from the imperial era with a rectangular plan and rounded corners. It occupies an area of 2.40 ha, although the area of interest (AOI) on which this work focuses is limited to a smaller area in which the defensive system with masonry walls are visible (Fig. 1, zones I and II).
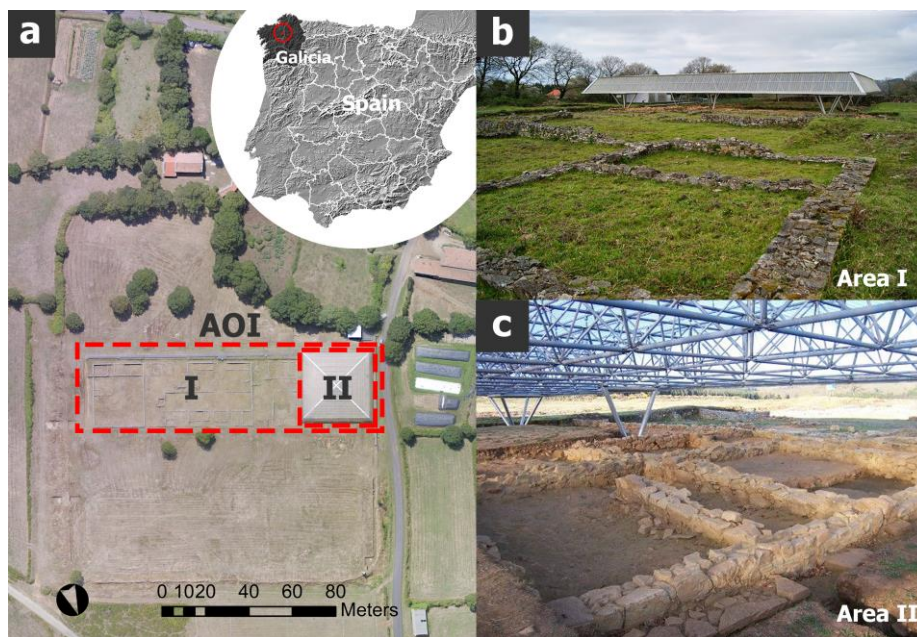
Fig. 1. Roman camp of *A Cidadela*. a) Location and general view of the camp: b) outside area (I) and c) area roof protective cover (II).

From a photogrammetric survey perspective, the main feature of this settlement is the existence of an auxiliary structure to protect the excavated area, which is very common in archaeological excavations. Artificial ceilings are used to protect structures and walls that have lost their "organic" character to become fragments with material conditions that are different from those they were originally designed for and used with, which makes them highly vulnerable to environmental conditions (Soria, Guerrero and García, 2017). However, these auxiliary structures typically pose challenges when modelling sites because they do not enable the acquisition of aerial UAV images, and they make the acquisition of pole images difficult if the height of the structure is not sufficient.

3.2   Field campaign and photogrammetric survey

Conventional SfM photogrammetry requires high overlap to ensure the generation of the model, while in hybrid photogrammetry (i.e., the combination of multisource imagery), the level of overlap is even more important, especially in the common zone between blocks. Therefore, the planning and image acquisition steps should be performed using geometric constraints of good spatial intersection and overlap. The overlap for this case study (i.e., 70% and 80% across and along the track, respectively) was defined in the prior planning phase to obtain good results in the dense matching process.

In August 2015, a flight was conducted using a vertical take-off and landing (VTOL) rotating-wing DJI Phantom 3 UAV (www.dji.com). The device weighs 1,280 g and has a specific gimbal to stabilize its integrated camera. The drone's camera incorporates a 6.16 × 4.62 mm (1/2.3) CMOS sensor that can capture 12.4-Mp images (4,000 × 3,000 pixels). The ground control station and the UAV were radio-linked and transmitted altitude, position and status data. To achieve a ground sample distance (GSD) less than 1 cm, the defined flight height was 26 m.

6

The digital single-lens reflex (DSLR) camera used for the area under the roof was a Canon EOS 550D with a 22.3 × 14.9 mm 18-megapixel CMOS sensor (5,184 × 3,456 pixels) with a pixel size of 4.3 × 4.3 μm. To improve the measurement quality of the model, a Canon EF 20-mm f/2.8 fixed focal length lens was used. This camera provides higher quality images than the one integrated in the UAV. To elevate the camera, it was necessary to employ a pole and use a first-person view system (FPV glasses) wire connected with a remote shooting button. Table 1 and Fig. 2 summarize the data corresponding to the images of both areas.
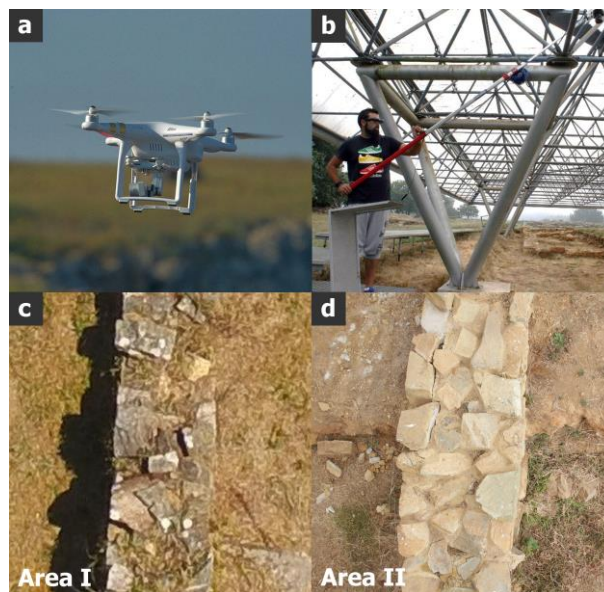

Fig. 2. Image capture systems: a) DJI Phantom 3 UAV, b) camera elevation with pole. Image samples of a wall showing the differences in GSD: c) drone image and d) DSLR image using the pole.

Table 1. Main characteristics of the datasets used

Area	Image resolution	# of images	Mean height	GSD
Area I	12.4 Mp	422	26.9 m	0.94 cm/pix
Area II	18 Mp	2,769	3.2 m	0.06 cm/pix

A Total Station was used to obtain GCPs and checkpoints in the outer and indoor areas. An overlap zone common to the area under the roof and aerial images was established

7

(approx. 3 m in width) along the edge of the roof to ensure image coupling. Figure 3a shows the location of the manually entered TPs that were used to test the influence of their use on the accuracy of the DSM.
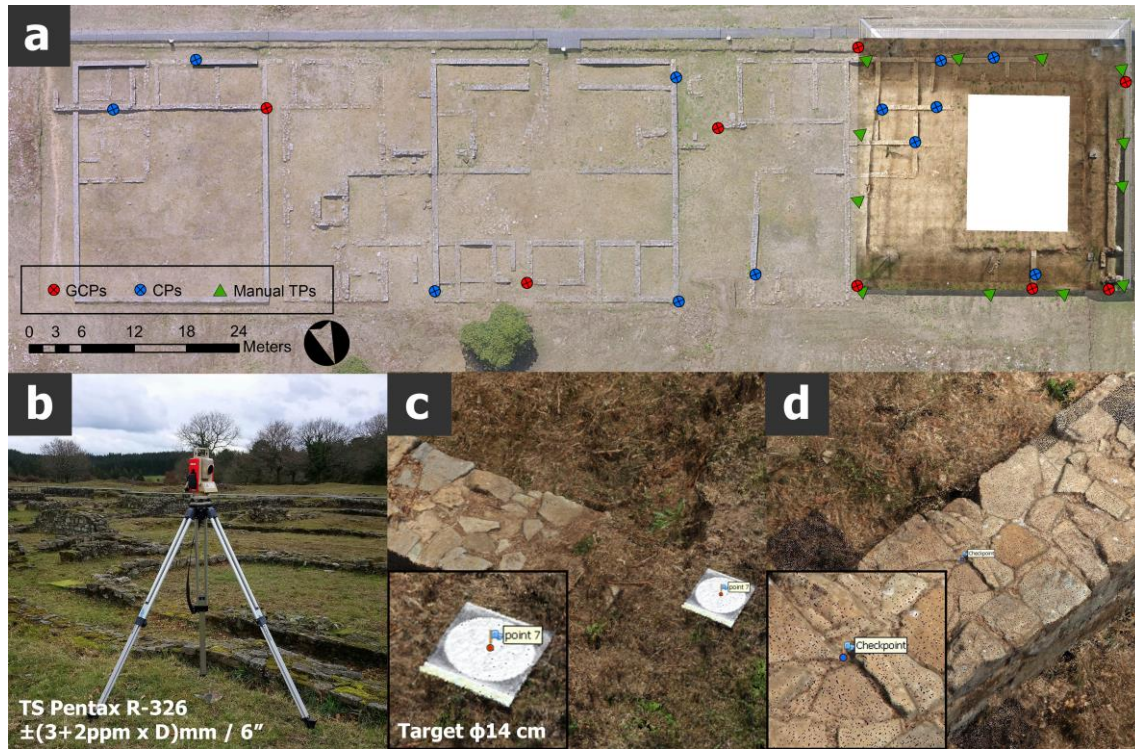

Fig. 3. a) Distribution of GCPs, checkpoints and manually entered TPs on the site; b) Total Station R-326 used to collect the points; c) GCPs identified with targets easily visible from the air; and d) checkpoints and TPs directly marked over clearly identifiable elements in the dense point cloud.

3.3 General workflow of hybrid photogrammetry

The general workflow of hybrid photogrammetry processing (Fig. 4) starts with the aforementioned planning phase of image acquisition. The planning must not only guarantee the desired GSD and a good overlap between the images of each block but also consider the zone of overlap between blocks. The 3D modelling process itself, using software based on SfM algorithms (Remondino *et al.*, 2017), involves the following steps: (1) automatic correlation, (2) hierarchical orientation, and (3) automatic

8

3D dense surface extraction. In stage (1), the software searches for common points on the photographs and matches them; it also finds the position of the camera for each image and refines the camera calibration parameters (2). As a result, a set of camera positions and a sparse point cloud are formed. Based on the estimated camera positions, the program calculates the depth information of each camera, which is combined into a single dense point cloud (3). The last steps of the process involve the generation of the mesh from the point cloud and the creation of the texture files, which produce the final DSM when combined.
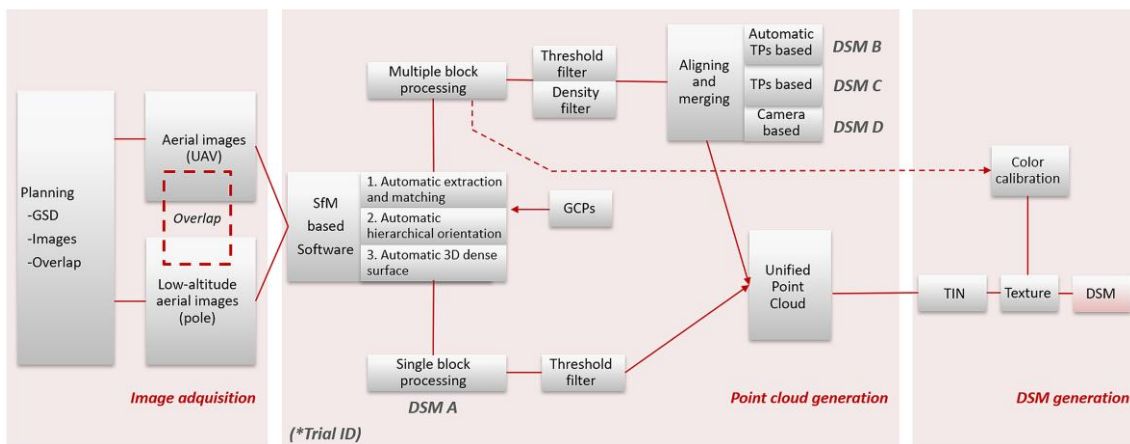
Fig. 4. General workflow of hybrid photogrammetry processing

Although SfM-based photogrammetry allows some flexibility in the geometry of the images, the geometries cannot be very different if orientation processing is performed simultaneously in a single block. In other cases, wide baselines can cause image alignment failures (Hidayat and Cahyono, 2016). To avoid this issue, common points that link both types of image blocks should be introduced. The introduction of GCPs before the hierarchical orientation and dense reconstruction processes is especially important when working with several different sensors and platforms.

Any SfM software requires a minimum of 3 GCPs to perform photogrammetric block adjustment, as well as scaling, rotating and locating the model. Each one of those points should be identified in at least two images. Although several studies have discussed this

issue (Goldstein *et al.*, 2015; Tonkin and Midgley, 2016), there is no distinct, accepted criterion for establishing the number of GCPs, and the determination depends on the size of the area. Tonkin and Midgley (2016) showed that 3 or 4 GCPs may result in acceptable levels of error within the quality range of the measurement source. We used the 8 GCPs indicated in Fig. 3a, which are defined based on circular white targets whose centroids can be easily and automatically extracted by the software. Some of the GCPs must be situated in the overlap area between the images from different sources.

Working with a **single block**, through the combined bundle adjustment, a more homogeneous photogrammetric point cloud is generally obtained, avoiding errors that would be obtained and propagated using a solid rigid transformation. In this case study, the combined bundle adjustment (UAV and low-altitude aerial imagery) is solved by the software using a least squares adjustment based on a collinearity equation (Torres-Martínez *et al.*, 2015):

$$x = x\left(\bar{c}_{pole}, \bar{c}_{uav}, \overline{eo}_{pole\,i}, \overline{eo}_{uav\,j}, \bar{X}_k\right) \qquad (1)$$

$$y = y\left(\bar{c}_{pole}, \bar{c}_{uav}, \overline{eo}_{pole\,i}, \overline{eo}_{uav\,j}, \bar{X}_k\right) \qquad (2)$$

where:

- $\bar{c}_{pole}$ and $\bar{c}_{uav}$ are the vectors of the cameras used for low-altitude aerial imagery and UAV imagery, respectively, which include the internal camera parameters (i.e., principal point coordinates and focal length) and lens distortion coefficients (radial-K, decentring-P and affinity parameters-b). Ten unknowns were used for each camera vector; $\bar{c} = (x_0, y_0, f, K_1, K_1, K_3, P_1, P_2, b_1,)$.

- $\overline{eo}_{pole\,i}$ and $\overline{eo}_{uav\,j}$ correspond to the six unknowns of the external orientation for low-altitude aerial imagery and UAV imagery, respectively. The external orientation vector is $\overline{eo} = (S_x, S_y, S_z, \omega, \varphi, \chi)$.

- $\bar{X}_k$ represents the spatial coordinates vector (X, Y, Z) of the unknown object points.

10

Although the collinearity equation is derived from the basic principles of classical photogrammetry, modern SfM software systems fully automate these procedures. The calculation of the parameters and the geometry of the camera are generally computed by the software through calibration routines in which the user does not interfere significantly (Chiabrando, Donadio and Rinaudo, 2015).

However, when **multiple blocks** must be used, and the data must be integrated to generate a single DSM, it is necessary to homogenize the information and establish filtering, simplification and optimization algorithms. As a useful initial approach for this homogenization of the blocks, it is necessary to adjust the density parameters of the software when generating each individual point cloud. Due to the varying GSD values of the images between zones I and II, the input parameters of the SfM process were adjusted independently for each of the two point cloud models. For the aerial model (I), the software configuration for the photo orientation and dense point cloud generation processes was set to "High", and for the covered area (II), the configuration was set to "Medium", which resulted in point clouds with densities of approximately 14,000 points/m^2 and 17,000 points/m^2, respectively.

To completely homogenize the point clouds in terms of point density, a spatial filtering of 0.7 cm was applied to the individual point clouds. Notably, the maximum size of filtering is limited by the resolution of the block with the highest GSD (in this case, the aerial survey). In addition, the GSD of the block with the poorest resolution provides a preliminary idea of the expected precision of a photogrammetric project (although the GSD can vary in close-range photogrammetry).

Once the point clouds are generated, filtering according to a distance threshold (5 m in this case) is recommended to remove distant points that exceed the limits of the pre-established AOI. Finally, the more delicate areas for the matching process (in our case, trees and the protective roof) were filtered and removed manually. It should be noted that the 3D modelling of the protective ceiling itself is of no interest in this case.

These previous steps and thresholds should be considered orientative and should be adapted by the user depending on the type and geometry of the area. The SfM software usually includes optimization algorithms and compresses the resulting clouds, which enables more efficient data storage.

The final steps in obtaining a DSM are triangulation of the mesh based on the point cloud and generation of its corresponding texture. Several methods can be used for triangulation; Delaunay triangulation is the simplest method implemented in almost all software packages (Lee and Schachter, 1980). The density of the polygonal mesh can be configured on the basis of the desired visual quality but also in relation to the scale of the survey. In this phase, artefacts or errors of definition often occur, probably due to the complexity of the scenario and, in particular, digital noise such as vegetation or elements that have not been eliminated from the point cloud.

Merging blocks prior to mesh calculation is ultimately more precise because the software works directly on photogrammetric data contained in the point cloud and thus determines each marker position accurately (Palestini and Basso, 2017). However, if the program has already elaborated a continuous three-dimensional surface, it may generate polygonal interpolation errors, and pattern matching may fail during the meshing phase.

The meshes can be then textured from the input images to generate a photorealistic representation of the scene. The texturization of the DSM in cases of hybrid photogrammetry, in which the images are from several different platforms and cameras, may require a radiometric adjustment to improve the visual quality of the final model and avoid abrupt radiometric changes in texture. In addition to the sensors, the lighting conditions may change significantly during the capturing scenario. In these cases, the homogenization of the brightness and white balance levels over the whole dataset is usually useful to avoid discontinuity artefacts. Photogrammetric processing software usually includes options for this purpose, although any independent batch image processor could be used instead. Seamlines are particularly susceptible areas for

12

artefacts to become visible; thus, quality checks are necessary in hybrid photogrammetry. The programs provide a wide range of tools to solve these problems (set texture colourisation method, modify lighting, manually assign the image or images to texture an indicated part of the model, etc). Thus, the final textured model can be improved visually according to user requirements.

3.4   Block alignment methods: Accuracy assessment

Obtaining a complete DSM of the entire archaeological complex of *A Cidadela* involved the photogrammetric processing of 3,191 images. Due to the relatively large size of the dataset and the various image sources, processing was divided into two blocks corresponding to areas I and II; several methods were applied to align the blocks. Alignment procedures allow for the coupling of blocks through solid rigid transformations in which the internal alignment of each block is not affected. To assess the results comparatively, the procedure was conducted in a unified manner by processing as a single block. Specifically, for this work, we used the software PhotoScan, as it probably offers the largest range of methods for block alignment. (1) The first method is point-based alignment, which aligns blocks by matching photos across all initial blocks. (2) The second method, which is incorporated in the majority of software packages (e.g., Pix4D), is based on user-entered markers (manually entered TPs as well as common GCP). (3) The third method is the camera-based alignment method, which is based on the precomputed locations of the common cameras. The image processing experiments of the case study dataset are shown in Table 2. All models were generated using a PC with a 2.80-GHz Intel Core i7-7700HQ, 32-GB RAM and an 8-GB NVIDIA GeForce GTX 1070 running PhotoScan Professional Edition version 1.4.1.

Table 2. Experimental design to test block alignment methods.

Trial code	Alignment type	GCPs	Observations
DSM A	Single block (no alignment required)	8 GCPs	
DSM B	Point-based	8 GCPs (5 GCPs per block with 2 located in the common area)	Block alignment based on dense point cloud matching
DSM C.1	Marker-based	8 GCPs (5 GCPs per block with 2 located in the common area)	4 TPs manually entered in the overlap area
DSM C.2			8 TPs manually entered in the overlap area
DSM C.3			12 TPs manually entered in the overlap area
DSM D	Camera-based	8 GCPs (5 GCPs per block with 2 located in the common area)	Block alignment based on 24 common cameras

An independent accuracy assessment based on the distances between check points in both blocks was conducted after model alignment and merging. To avoid the influence of the imprecision of point marking, the checkpoints that define the distances were previously marked in the individual blocks and imported automatically during the fusion process. Because the alignment and merging processes only modified the positions of one of the models, the coordinates of the checkpoints in the base block were not modified. In all tests, we considered block I as the base block and block II as the block that was aligned.

4 Results and Discussion

4.1 Field campaign and photogrammetric survey

To cover the total AOI of the archaeological site (4,000 m^2), 4 25-minute flights were conducted, and 422 photographs were taken for the entire exterior area (area I). On the same day, the ground campaign was conducted in the area beneath the roof (approx. 900 m^2). In this area (area II), the supporting structure did not allow the use of the UAV. Thus, it was necessary to employ a pole to elevate the camera using a remote vision and shooting system due to the maximum ceiling height (3.00–3.40 m). To ensure an equivalent overlap with the aerial survey, a large number of photographs were taken (i.e., 2,769 images with a mean height of 3.19 m). Although the structural bars of the ceiling were an occlusive element that made it even more difficult to obtain images and inevitably reduced the usable surface of the photographs, the structural elements of the roof were used to stabilize the camera shots by supporting the pole to achieve less blurry images.

The GSD of the images was likely the most important factor to determine the accuracy of the DSM. The photographs of the two blocks were planned to ensure GSD values of less than 1 cm in all cases. Since the AOI is relatively flat and free of obstacles, and the flight conditions were good, the aerial survey did not have difficulty reaching the longitudinal and transversal overlap (70%/80%) according to the planned parameters. In area II (beneath the roof), ensuring an equivalent overlap resulted in labour-intensive image acquisition. We can independently compare the yields of the aerial and terrestrial techniques in the study area (0.105 img/m^2 and 3.076 img/m^2, respectively) based on the number of photographs that were necessary to model 1 m^2 of land.

15

4.2 General workflow of hybrid photogrammetry

The DSMs for each area (Fig. 5) were generated following the described workflow. The estimated positions of the GCPs in the DSMs generated for areas I and II clearly differ in terms of the root mean square error (RMSE) of the adjustment of the models (Table 3), mainly due to the differences in the achievable ground resolutions. In the aerial images (I), a dense point cloud with 9.330 mm/pix was generated, which contrasts the 0.602 mm/pix in the area under roof (II). As this method of quality checking neither requires nor uses independent measurements, the value should be analysed in terms of internal precision rather than overall accuracy.
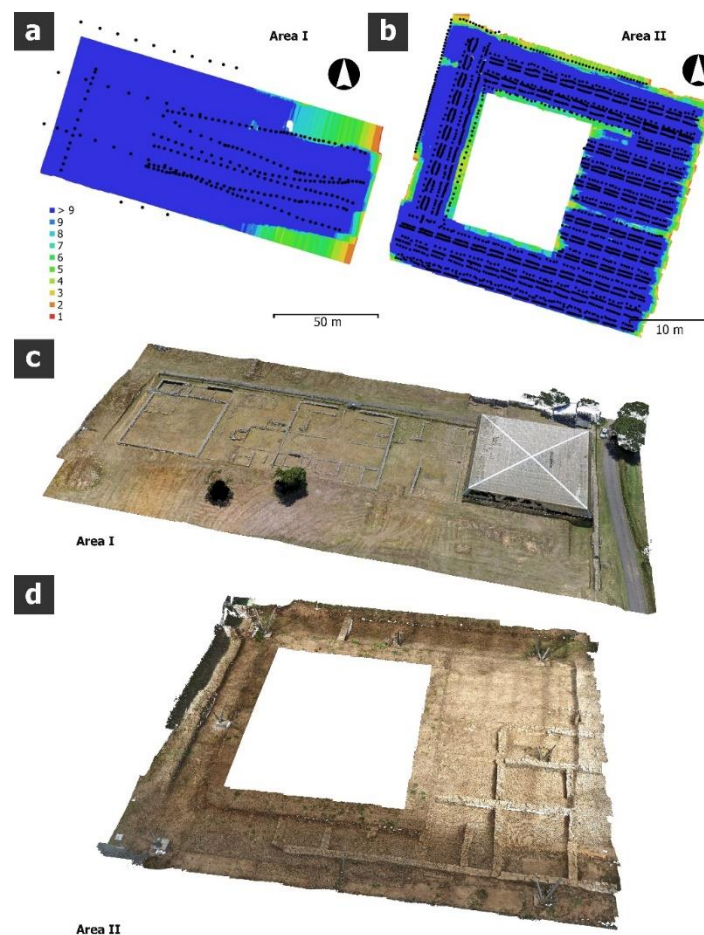
Fig. 5. Image positions (black dots) and number of overlapped images in both areas of the archaeological site: a) outside area (I) and b) area under protective cover (II). Dense point clouds generated for: c) the outside area (I) and d) the area under protective cover (II). The unmodelled

16

central area corresponds to a flat unexcavated area, which was not included because it has no archaeological interest. Complete 3D available in Sketchfab: https://skfb.ly/6zG7r.

Table 3. RMSE values based on GCP adjustment.

	RMSE X (cm)	RMSE Y (cm)	RMSE Z (cm)	Total RMSE (cm)
DSM - Area I (UAV)	1.5572	2.5004	3.2200	4.3641
DSM - Area II (pole)	11.3050	6.0361	13.3609	18.5135
Single Block DSM – Entire Area	6.2587	8.3401	19.2046	21.8528

4.3 Block alignment methods: Accuracy assessment

When processing a single block, the SfM software uses whatever constraints it has (coordinates of GCPs, TPs, fix distances and pre-calibrated camera parameters) to optimize the sparse point cloud, camera spatial positions, and orientations and improve camera calibration. By removing certain constraints (such as poor TPs), the alignment result is optimized (a new "best-fit" model is calculated by bundle adjustment), and the overall accuracy is increased. In the case of a single block, all of these constraints are linked because they have been compared through a simultaneous adjustment and the TPs (generally the most important constraint in SfM photogrammetry) form a single interlinked whole. The bundle adjustment based on the collinearity equation allows for different cameras to be oriented in a single process because the calibration parameters can be calculated for subgroups of images in the same block or for each image individually. The results (Fig. 6) show that the overall accuracy of the DSM can be significantly higher using the same GCPs in single-block processing (3.77-cm RMSE) because it avoids propagating block alignment errors. The total time does not significantly differ from that required to process blocks separately and to perform the alignment and fusion. Thus, conducting single-block processing is recommended but

limited by the DSM size and the capacity of the computer to compute the batch of images simultaneously.
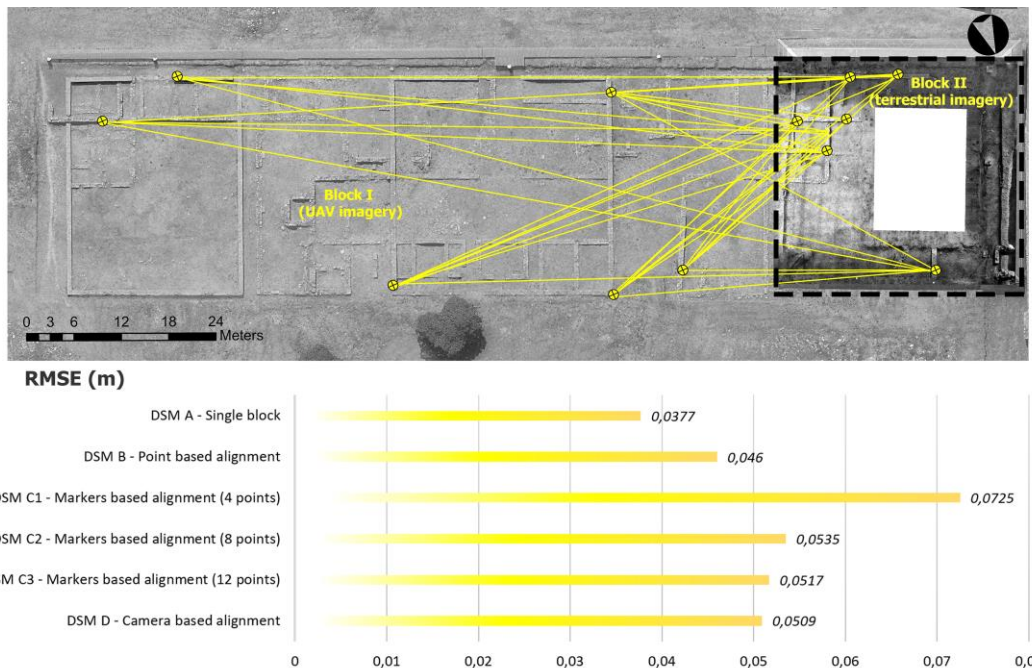
Fig. 6. Accuracy assessment with the distances between checkpoints in both blocks. The graph compares the RMSE values of each trial.

When a point-based alignment operation is used, SfM software starts the image-matching process for images from all blocks being aligned. This method is the most time-intensive alignment method because it requires the analysis of the two dense point clouds in search of common points. The TPs found are exclusively used in the block alignment and are discarded after the operation.

In the case of marker-based alignment, when a block is being aligned with another reference block, the estimated marker coordinates of the reference block are used. The union of multiple consecutive blocks exclusively using markers can lead to additional accumulated errors. Therefore, this alignment method is recommended only when adequate marker accuracy can be guaranteed. The number of markers must also be sufficient to guarantee that the program can optimize the new position of the block

18

using least squares. Based on the distance accuracy assessment, adding 8 to 12 well-distributed, manually entered TPs in the overlap area can notably improve the accuracy of the DSM.

The alignment of blocks using the camera-based method requires working with blocks that share common photographs. The accuracy assessment shows similar results with regard to alignment using cameras and points (5.09-cm RMSE and 4.60-cm RMSE, respectively). However, the camera method takes a few seconds rather than the up to 6 hours required for the point-based method. Including common photographs at the boundary between blocks in each is essential for alignment using the camera method and is also important for TP generation when using point-based alignment.

5   Conclusions

Integrated 3D modelling using different platforms is expected to contribute to digital documentation technology for the spatial analysis of complex archaeological sites. However, good planning of the areas of overlap when taking photographs is essential to ensure the completeness and accuracy of the DSM.

The varying ground resolution of images can be partially addressed using simplification and filtering algorithms to homogenize the data. For that matter, programs used in photogrammetry often provide solutions for homogenizing textures to achieve more uniform results.

When working with large datasets that exceed the processing capabilities of the equipment, or when it is necessary to add an extra set of images to an already processed project, multiple blocks may be required. In those cases, correct block alignment is critical when attempting to construct a single point cloud. The point-based alignment method yields better results in terms of accuracy because it uses a higher number of TPs derived from a new matching process between the point clouds. In contrast, marker-

based and camera-based methods perform block alignment more quickly. Camera-based alignment requires some common photographs between adjacent blocks; clearly identifiable points should be used when using entered markers as TPs because it requires high precision to add points in both blocks. Based on the results, the number of TPs should be approximately 8. Adding more TPs does not notably improve the accuracy, and it can be a time-consuming task to identify a higher number of points over the common area of the blocks to be merged. Notably, drawing conclusions about the alignment with markers based on the above tests may not be appropriate because this practical case is too simple with regard to the number of "chunks" (only two blocks). Further studies should focus on the analysis of the possible accumulation of errors when multiple consecutive blocks are aligned.

Acknowledgements

6   References

Arif, R. and Essa, K. (2017) 'Evolving techniques of documentation of a world heritage site in Lahore', in *The International Archives of the Photogrammetry, Remote Sensing and Spatial Information Sciences, 26th International CIPA Symposium 2017*. Ottawa,

Canada, pp. 33–40. doi: 10.5194/isprs-archives-XLII-2-W5-33-2017.

Bemis, S. *et al.* (2014) 'Ground-based and UAV-Based photogrammetry : A multi-scale , high- resolution mapping tool for structural geology and paleoseismology', *Journal of Structural Geology*. Elsevier Ltd, 69, pp. 163–178. doi: 10.1016/j.jsg.2014.10.007.

Bermejo, L. *et al.* (2018) 'Assessing the accuracy of 3D GPR results by comparing them to 3D laser scanner models : the case study of the archaeological site of Peluda Cave (Sierra de Atapuerca , Burgos , Spain)', in *Geophysical Research Abstracts. EGU General Assembly 2018*.

Bolognesi, M. *et al.* (2014) 'Accuracy of Cultural Heritage 3D Models by RPAS and Terrestrial Photogrammetry', in *ISPRS Technical Commission V Symposium*. Riva del Garda, Italy ACCURACY: The International Archives of the Photogrammetry, Remote Sensing and Spatial Information Sciences, pp. 23–25. doi: 10.5194/isprsarchives-XL-5-113-2014.

Campana, S. (2017) 'Drones in Archaeology. State-of-the-art and Future Perspectives', *Archaeological Prospection*, 24(4), pp. 275–296. doi: 10.1002/arp.1569.

Chiabrando, F., Donadio, E. and Rinaudo, F. (2015) 'SfM for orthophoto generation: Awinning approach for cultural heritage knowledge', *International Archives of the Photogrammetry, Remote Sensing and Spatial Information Sciences - ISPRS Archives*, 40(5W7), pp. 91–98. doi: 10.5194/isprsarchives-XL-5-W7-91-2015.

Field, S., Waite, M. and Wandsnider, L. (2017) 'The utility of UAVs for archaeological surface survey: A comparative study', *Journal of Archaeological Science: Reports*. Elsevier, 13(April), pp. 577–582. doi: 10.1016/j.jasrep.2017.05.006.

Fugazza, D. *et al.* (2018) 'Combination of UAV and terrestrial photogrammetry to assess rapid glacier evolution and map glacier hazards', *Natural Hazards and Earth System Sciences*, 18, pp. 1055–1071.

Goldstein, E. *et al.* (2015) 'Ground control point requirements for structure-from-motion derived topography in low- slope coastal environments', *PeerJ PrePrints*. doi:

10.7287/peerj.preprints.1444v1 |.

Green, S., Bevan, A. and Shapland, M. (2014) 'A comparative assessment of structure from motion methods for archaeological research', *Journal of Archaeological Science*. Elsevier Ltd, 46(1), pp. 173–181. doi: 10.1016/j.jas.2014.02.030.

Hidayat, H. and Cahyono, A. (2016) 'Combined aerial and terrestrial images for complete 3D documentation of Singosari Temple based on Structure from Motion algorithm', in *IOP Conference Series: Earth and Environmental Science*. IOP Publishing, pp. 0–11. doi: 10.1088/1755-1315/47/1/012004.

Lee, D. T. and Schachter, B. J. (1980) 'Two algorithms for constructing a Delaunay triangulation', *International Journal of Computer & Information Sciences*, 9(3), pp. 219–242. doi: 10.1007/BF00977785.

Manferdini, A. M. and Galassi, M. (2013) 'Assessment for 3D Reconstructions of Cultural Heritage using Digital Technologies', *ISPRS - International Archives of the Photogrammetry, Remote Sensing and Spatial Information Sciences*, XL-5/W1(Feb), pp. 167–174. doi: 10.5194/isprsarchives-XL-5-W1-167-2013.

Martínez-Carricondo, P. *et al.* (2018) 'Assessment of UAV-photogrammetric mapping accuracy based on variation of ground control points', *International Journal of Applied Earth Observation and Geoinformation*. Elsevier, 72(May), pp. 1–10. doi: 10.1016/j.jag.2018.05.015.

Nocerino, E. *et al.* (2013) 'Accuracy and block deformation analysis in automatic UAV and terrestrial photogrammetry - lesson learnt', in *ISPRS Annals of the Photogrammetry, Remote Sensing and Spatial Information Sciences, XXIV International CIPA Symposium*. Strasbourg, France, pp. 2–6. doi: 10.5194/isprsannals-II-5-W1-203-2013.

Palestini, C. and Basso, A. (2017) 'Geomatics as a survey tool to document and enhance the cultural and landscaped heritage of the monumental complexes in the mountains of Abruzzo', in *The International Archives of the Photogrammetry, Remote Sensing and Spatial Information Sciences, 2017 GEOMATICS & RESTORATION – Conservation of*

Cultural Heritage in the Digital Era. Florence, Italy, pp. 373–380. doi: 10.5194/isprs-Archives-XLII-5-W1-373-2017.

Remondino, F. *et al.* (2013) 'Dense image matching: Comparisons and analyses', in *Proceedings of the DigitalHeritage 2013 - Federating the 19th Int'l VSMM, 10th Eurographics GCH, and 2nd UNESCO Memory of the World Conferences, Plus Special Sessions fromCAA, Arqueologica 2.0 et al.*, pp. 47–54. doi: 10.1109/DigitalHeritage.2013.6743712.

Remondino, F. *et al.* (2017) 'A critical review of automated photogrammetric processing of large datasets', in *The International Archives of the Photogrammetry, Remote Sensing and Spatial Information Sciences, 26th International CIPA Symposium 2017*. Ottawa, Canada, pp. 591–599. doi: 10.5194/isprs-archives-XLII-2-W5-591-2017.

Robleda, P. G. *et al.* (2015) 'Modeling and accuracy assessment for 3D-virtual reconstruction in cultural heritage using low-cost photogrammetry: Surveying of the "santa maría azogue" church's front', *International Archives of the Photogrammetry, Remote Sensing and Spatial Information Sciences - ISPRS Archives*. Elsevier B.V., 40(5W4), pp. 263–270. doi: 10.5194/isprsarchives-XL-5-W4-263-2015.

Sapirstein, P. (2016) 'Accurate measurement with photogrammetry at large sites', *Journal of Archaeological Science*. Elsevier Ltd, 66, pp. 137–145. doi: 10.1016/j.jas.2016.01.002.

Seibert von Fock, S. *et al.* (2017) 'Pipeline for Reconstruction and Visualization of Underwater Archaeology Sites using Photogrammetry Reconstruction Image Processing', in *32nd International Conference on Computers and Their Applications*. Honolulu.

Senol, H. I. *et al.* (2017) '3D Modeling of a Bazaar in Ancient Harran City Using Laser Scanning Technique', in *4th International GeoAdvances Workshop*. Karabuk, Turkey: The International Archives of the Photogrammetry, Remote Sensing and Spatial Information Sciences, pp. 99–101. doi: 10.5194/isprs-archives-XLII-4-W6-99-2017.

Soria, F. J., Guerrero, L. F. and García, A. B. (2017) 'Protective Roof Systems for

Archeological Sites in Mexico', *WIT Transactions on The Built Environment*, 171, pp. 225–236. doi: 10.2495/STR170201.

Tonkin, T. and Midgley, N. (2016) 'Ground-Control Networks for Image Based Surface Reconstruction : An Investigation of Optimum Survey Designs Using UAV Derived Imagery and Structure-from-Motion Photogrammetry', *Remote Sensing*, 8(786), pp. 16–19. doi: 10.3390/rs8090786.

Torres-Martínez, J. A. *et al.* (2015) 'A Multi-data source and multi-sensor approach for the 3d reconstruction and visualization of a complex archaelogical site: The case study of tolmo de minateda', *International Archives of the Photogrammetry, Remote Sensing and Spatial Information Sciences - ISPRS Archives*, 40(5W4), pp. 37–44. doi: 10.5194/isprsarchives-XL-5-W4-37-2015.

Tscharf, A. *et al.* (2015) 'On the Use of Uavs in Mining and Archaeology - Geo-Accurate 3D Reconstructions Using Various Platforms and Terrestrial Views', *ISPRS Annals of Photogrammetry, Remote Sensing and Spatial Information Sciences*, II-1/W1, pp. 15–22. doi: 10.5194/isprsannals-II-1-W1-15-2015.

Westoby, M. J. *et al.* (2012) '"Structure-from-Motion" photogrammetry: A low-cost, effective tool for geoscience applications', *Geomorphology*. Elsevier B.V., 179, pp. 300–314. doi: 10.1016/j.geomorph.2012.08.021.